

Effat University Repository

A Novel PAPR in OTFS Systems through ISSA-PTS and ISPR Techniques

Authors	Hussein, Aziza;A. A., Mohamed;Mabrook, M. Mourad
Citation	G. M. Salama, A. A. Mohamed, A. I. Hussein and M. Mourad Mabrook, "A Novel PAPR in OTFS Systems through ISSA-PTS and ISPR Techniques," in IEEE Access, https://doi.org/10.1109/ACCESS.2024.3487960
DOI	10.1109/ACCESS.2024.3487960
Publisher	IEEE
Download date	2026-04-17 22:41:32
Link to Item	http://hdl.handle.net/20.500.14131/1979

Received 7 October 2024, accepted 24 October 2024, date of publication 30 October 2024, date of current version 27 November 2024.

Digital Object Identifier 10.1109/ACCESS.2024.3487960

RESEARCH ARTICLE

A Novel PAPR in OTFS Systems Through ISSA-PTS and ISPR Techniques

GERGES MANSOUR SALAMA¹, AMIRA A. MOHAMED^{1,2},
AZIZA I. HUSSEIN³, (Member, IEEE), AND M. MOURAD MABROOK⁴

¹Electrical Communications Engineering Department, Faculty of Engineering, Minia University, Minia 61111, Egypt

²Department of Electronics and Electrical Communications, Higher Institute of Engineering and Technology, Kafr El-Shaikh 33511, Egypt

³College of Engineering, Energy and Technology Research Center, Effat University, Jeddah 22332, Saudi Arabia

⁴Space Communication Department, Faculty of Navigation Science and Space Technology, Beni-Suef University, Beni-Suef 62511, Egypt

Corresponding author: Amira A. Mohamed (amira.alshoraky2@gmail.com)

ABSTRACT In modern communication systems, managing the Peak-to-Average Power Ratio (PAPR) remains a critical challenge, particularly in Orthogonal Time-Frequency Space (OTFS) systems. PAPR significantly influences the efficiency and performance of these systems, with high PAPR leading to signal distortion and reduced system reliability. This is especially problematic in high-speed mobility environments, such as high-speed railway systems, where OTFS modulation is favored for its robustness in dispersive channels. However, the high PAPR in OTFS systems can compromise the performance of power amplifiers, increasing signal distortion and Bit Error Rate (BER). This study introduces two novel PAPR reduction techniques: a hybrid approach combining the Improved Salp Swarm Algorithm (ISSA) with Partial Transmit Sequence (PTS) and an innovative Iterative Sub-block Phase Rotation (ISPR) method. The hybrid ISSA-PTS approach optimizes phase rotations to reduce PAPR, while the ISPR technique further enhances PAPR reduction by iteratively rotating sub-block phases without compromising BER. Simulation results demonstrate that both proposed techniques significantly reduce PAPR and improve BER performance, making them promising solutions for enhancing the reliability and efficiency of OTFS systems in high-mobility communication environments.

INDEX TERMS OTFS, PAPR, high-speed mobility, OFDM, delay-Doppler domain, ISPR, ISSA, BER.

I. INTRODUCTION

Managing the PAPR remains a critical challenge in modern communication systems, particularly in Orthogonal Time-Frequency Space (OTFS) systems [1]. PAPR is a crucial parameter that influences the efficiency and performance of communication systems [2]. High PAPR can lead to significant signal distortion and reduced system reliability. It is imperative to address this issue to optimize communication performance and ensure the successful deployment of advanced modulation schemes [3].

The rapid growth of high-speed mobility, particularly in high-speed railway systems, has led to a surge in traffic flow and the widespread adoption of vehicle-mounted

communication systems [4]. As a result, there is growing attention on enhancing wireless communication technologies in high-mobility environments, and satellite. OTFS is a promising modulation technique for high-frequency, high-latency communication settings [5]. Known for its resilience in dispersive channels, OTFS offers improved data transmission reliability. However, a significant drawback of OTFS systems is the high PAPR associated with their signals, leading to inefficiencies in power amplification and potential signal degradation [6].

Addressing the high PAPR in OTFS systems is crucial for advancing their practical application [7], [8], [9]. Extensive research has focused on developing effective PAPR reduction techniques. In this study, two systems have been proposed, hybrid the two sophisticated optimization techniques: the Improved Salp Swarm Algorithm (ISSA) and

The associate editor coordinating the review of this manuscript and approving it for publication was Prakasam Periasamy¹.

Partial Transmit Sequence (PTS). The ISSA, an advanced metaheuristic optimization algorithm, enhances the search for optimal phase rotations, while PTS adds a layer of phase manipulation to reduce PAPR further. The integration of these techniques aims to create a robust solution for PAPR reduction in OTFS systems [9].

The novelty of the second technique lies in the innovative combination of Iterative Sub-block Phase Rotation (ISPR), forming a comprehensive framework for PAPR reduction. This hybrid approach leverages the strengths of each technique, offering a scalable and effective solution that not only improves the efficiency of PAPR reduction but also contributes to the advancement of communication technologies. While ISPR has shown promise in lowering PAPR while maintaining signal integrity, further optimization is necessary to enhance its effectiveness.

This study offers a significant contribution to the ongoing efforts to address PAPR challenges and enhance the reliability of modern communication systems.

The remainder of this study is structured as follows: Section II reviews related work in OTFS and PAPR reduction techniques. Section III provides a detailed overview of the OTFS system, including its PAPR expression. Section IV introduces the proposed systems, focusing on the first proposed system, hybrid ISSA with PTS in the OTFS system, and detailing the second proposed system, ISPR-OTFS. The simulation results, including an analysis of complexity, are presented in Section V. Section VI concludes the paper with a summary of the findings and potential future research directions.

II. RELATED WORK

OTFS modulation has emerged as a promising solution for high-frequency communication environments, particularly in scenarios characterized by high latency and significant Doppler shifts [10]. Unlike traditional Orthogonal Frequency Division Multiplexing (OFDM), which operates in the time-frequency domain, OTFS transmits information symbols in the delay-Doppler (DD) domain, transforming a doubly-dispersive channel into a nearly non-fading one, as demonstrated by Sui et al. in their low-complexity detection scheme for spatial modulation-aided OTFS systems operating in doubly-selective channels [11]. Despite its advantages, OTFS, like OFDM, suffers from the problem of high Peak-to-Average Power Ratio (PAPR), which can cause significant signal distortion and degrade system performance [12].

OTFS has gained attention for its ability to maintain consistent symbol performance across a data frame by leveraging the delay-Doppler (DD) domain, making it resilient to channel fading effects, as analyzed by Shi et al. in the context of integrated sensing and communication systems [13]. However, as with OFDM, OTFS systems are prone to high PAPR, particularly when the number of Doppler bins increases [14]. High PAPR poses a significant challenge as it can push the High Power Amplifier (HPA) into a

non-linear operating region, resulting in signal distortion and increased Bit Error Rate (BER), as discussed by Khalaf et al. in their study on non-linear companding techniques for PAPR reduction in OFDM [15]. Consequently, various PAPR reduction techniques have been developed, focusing on either signal distortion or multiple signaling and probabilistic methods [16], [17], [18], [19], [20], [21], [22], [23], [24], [25], [26], [27].

Partial Transmit Sequence (PTS) is a widely studied technique for PAPR reduction in OFDM and OTFS systems. It divides the signal into several sub-blocks, each phase rotated independently to minimize PAPR. While effective, PTS is computationally intensive and requires the transmission of side information, which can reduce overall spectral efficiency [3], [28]. PTS requires side information to be transmitted, adding to the system's complexity and reducing efficiency [28].

The integration of Particle Swarm Optimization (PSO) with PTS has been explored to reduce the computational complexity of the traditional PTS technique [29]. PSO with PTS optimizes the phase factors for each sub-block, effectively reducing PAPR while maintaining good BER performance [30]. This method has shown promise in OTFS systems, particularly in scenarios with large Doppler shifts, by efficiently segmenting 2D signals and optimizing PAPR reduction without excessive computational overhead.

The ISSA algorithm is a bio-inspired optimization technique that mimics the foraging behavior of salps [31]. In the context of OTFS, ISSA is used to optimize the phase rotation applied to sub-blocks in the PTS framework [32]. This approach reduces the computational complexity associated with traditional PTS while improving the performance of the PAPR reduction. ISSA-OTFS is particularly effective in scenarios with large Doppler shifts, where conventional methods struggle to maintain low PAPR without compromising the BER of the OTFS with ISPR. This novel technique enhances the traditional PTS approach by introducing iterative sub-block phase rotation. This method avoids the need for side information transmission and reduces the complexity of searching for the optimal phase sequence. By applying an iterative phase rotation strategy, ISPR-OTFS effectively reduces PAPR without degrading spectral efficiency or increasing system complexity. This makes it a promising solution for high-speed mobility environments deployed by OTFS systems.

III. OTFS SYSTEM

Figure 1 displays the block diagram of an OTFS system.

There are two 2D transformations in it. The information symbol $x_{dd}[n, m]$ in the DD domain is first mapped by the transmitter to $x_{tf}[l, k]$ in the TF domain. The inverse symplectic finite Fourier transform (ISFFT) and windowing implement the OTFS transformation. Subsequently, the Heisenberg transform is used to transform $y_{tf}[l, k]$ from the TF domain to the time domain as the signal $X(t)$ and then sent through the channel [3]. On the receiver side, the

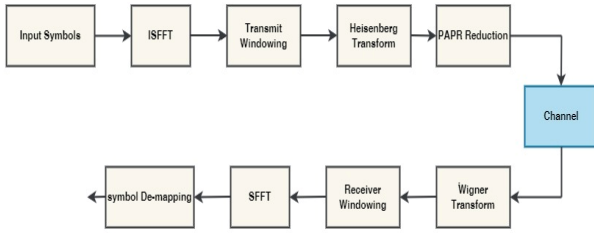


FIGURE 1. OTFS PAPR system model.

operations opposite to those done on the time-domain signal $Y(t)$ are performed, which is then transformed by the Wigner transform (inverse of Heisenberg transform) to get the TF domain symbol $y_{tf}[l, k]$. The symbols of the TF domain are then transformed into the DD domain with the help of the SFFT to get $y_{dd}[n, m]$. However, before $X(t)$ is transmitted over the wireless channel it needs to be amplified using the power amplifier [28]. The amplifier's linear range must be sufficiently comprehensive for a high PAPR. Otherwise, there would be distortion in the transferred data.

Assume that the total duration of the transmitted OTFS signal is $N \times T$, and the bandwidth occupied by the transmitted signal is $= \Delta f \times M$. The transmitted signal information is represented in the DD domain as $x_{dd}[n, m]$, $n = 0, 1, \dots, N - 1, m = 0, 1, \dots, M - 1$. And $x_{tf} \in \mathcal{Q}$ where represents QAM modulation where \mathcal{Q} represents QAM modulation constellations, which are regarded as grids within the 2D Doppler grids. These symbols can be mapped to symbols in the TF domain by ISFFT, which is [3]:

$$x_{tf}[l, k] = \sum_{n=0}^{N-1} \sum_{m=0}^{M-1} x_{dd}[n, m] \cdot e^{-i2\pi(\frac{km}{M} - \frac{ln}{T})} \quad (1)$$

Through the Heisenberg transform [3], the TF domain signal can be converted into the time-domain signal, which is given by:

$$x(t) = \sum_{n=0}^{N-1} \sum_{m=0}^{M-1} x_{tf}[l, k] p_{tx} \cdot e^{-i2\pi k v_f(t-NT)} \quad (2)$$

where p_{tx} represents the periodic pulse signal with a duration of $N \times T$. Through Nyquist sampling with a sampling rate of $F_s = \frac{1}{T_s} = B$, $s(t)$ becomes:

$$x(uTs) = \sum_{l=0}^{N-1} \sum_{k=0}^{M-1} x_{tf}[l, k] p_{tx}(uTs - nT) \times e^{-j2\pi kf(uTs - lT)} \quad (3)$$

where $u = 0, 1, \dots, MN - 1$, substitute $u = k + iM$, where $j = 0, 1, \dots, M - 1, i = 0, 1, \dots, N - 1$ it can be obtained as:

$$x(j + iM) = M \sum_{l=0}^{N-1} \tilde{x}_j[l] p_{tx}([j + iM - lM]_{MN}) \quad (4)$$

where $\tilde{x}_j[l] = \sum_{m=0}^{N-1} x[m, j] e^{\frac{j2\pi ln}{N}}$

Equation (4) is the transmission sample of the OTFS signal. According to [16], the PAPR of a frame of discrete OTFS transmission signal is:

$$PAPR = \frac{\max(j, i) |x(j + iM)|^2}{P_{avg}} \quad (5)$$

where $P_{avg} = \frac{1}{MN} \sum_{j=0}^{M-1} \sum_{i=0}^{N-1} E\{|s(j + iM)|^2\}$

The PAPR upper bound of the transmitted OTFS signal is [16]:

$$PAPR_{max} = \frac{N |\max[n, m]|^2}{\sigma^2} \quad (6)$$

where $\sigma^2 = E\{|[n, m]|\}^2$

The complementary cumulative distribution function (CCDF) is utilized to examine the PAPR of OTFS signals. The following Equation, where $PAPR_0$ is the presumed threshold, gives the likelihood that the Peak Average Power Ratio (PAPR) will not exceed the threshold, according to [16]:

$$P(PAPR \leq PAPR_0) \approx (1 - e^{-PAPR_0}) \quad (7)$$

Equation (8) represents the likelihood that the PAPR of the OTFS signal delivered in each frame will not exceed λ_0 when the Nyquist sampling ratio is 1, assuming that all OTFS signals are uncorrelated. Reference [18] states that when the sent signal is oversampled in a multi-carrier modulation, the assumption that the transmitted signal samples are uncorrelated is invalid. As a result, the OTFS signal PAPR's CCDF is described as follows:

$$P(PAPR \leq PAPR_0) \approx 1 - (1 - e^{-PAPR_0})^{MN} \quad (8)$$

IV. PROPOSED SYSTEMS

The input data blocks of N symbols are initially partitioned into M disjoint sub-blocks in the PTS method. Further, IFFT is carried out separately for every sub-block and then weighted by the phase ors $b_m = \exp(j\varphi_m)$ ($\varphi_m = [0, 2\pi], 1 \leq m \leq M$). In the OTFS systems, the PFs are chosen to minimize the PAPR value of the OTFS signals in all the sub-blocks. The primary b_m objective of this study is to choose the OPFs, denoted by \tilde{b}_m which reduces the PAPR value of the combined signals x_m where x is mathematically denoted [19], the OPFs are selected to minimize the PAPR value, and it is described as follows:

$$x = \sum_{k=1}^M \tilde{b}_k x_k \left[\tilde{b}_1, \tilde{b}_2, \dots, \tilde{b}_k \right] \arg \min(\max \left| \sum_{k=1}^M b_k x_k \right|) \quad (9)$$

The signals with lower PAPR values are mathematically expressed as:

$$x = \sum_{k=1}^M \tilde{b}_k x_k \quad (10)$$

However, an exhaustive search is required to select OPFs, which usually results in higher computational complexity. Generally, the selection of OPFs is limited to a b_m set of elements $b = \{\pm i, \pm j\}$ that efficiently reduce the search complexity. In this scenario, sets of PFs need to be searched 4^M for finding the OPFs. The search complexity is increased due to more sub-blocks, and the performance of the PTS method in PAPR reduction is wholly based on the total number of sub-blocks.

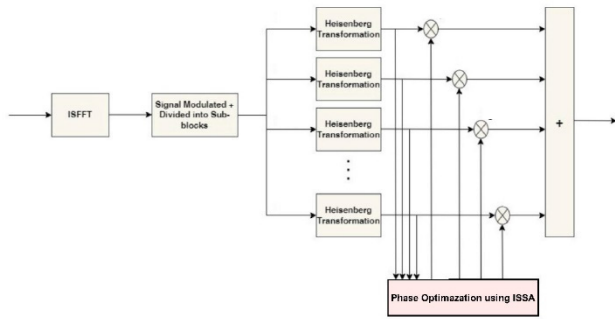


FIGURE 2. Flow diagram of the PTS-ISSA for the OTFS model.

A. FIRST PROPOSED SYSTEM (PTS-ISSA-OTFS)

A schematic of the PTS-ISSA is shown in Fig. 2.

The conventional SSA is an effective swarm intelligence-based optimization algorithm that mimics salps’ chain movement behavior. Generally, the salps are divided into two types leaders and followers [31]. The salps at the front of the chain are considered leaders, and the residual salps are followers. The leader guides the swarm directly or indirectly, and the followers follow each other. Like other optimization algorithms, the salps’ positions are determined in a d dimensional search space. As mentioned above, the leader salps are positioned at the front of the chain to explore the location of food sources [32]. Iteratively, the salps update their positions or places, which are calculated by the mathematical expression:

$$x_j^1 = \begin{cases} F_j + c_1 ((ub_j - lb_j) c_2 + lb_j) & c_3 \geq 0 \\ F_j - c_1 ((ub_j - lb_j) c_2 + lb_j) & c_3 < 0 \end{cases} \quad (11)$$

where the upper and lower bounds are denoted as ub_j and lb_j , c_1 is indicated as a coefficient value, which is vital in balancing the exploration and exploitation abilities, c_2 and c_3 are two independent random numbers that range between zero to one, F_1 is represented as the location of the food sources, and x_j^1 is denoted as the position of the 1st salps in a d dimensional search space. In the conventional SSA, the coefficient value c_1 decreases non-linearly from two to zero, as follows:

$$c_1 = 2e^{(-\frac{4l}{L})^2} \quad (12)$$

where the term l is indicated as the present iteration number, and L is represented as the maximum iteration. The follower’s salps L move with the leader’s salp, after updating the position of the followers, and this process is mathematically expressed in the following Equation:

$$x_j^i = \frac{1}{2}at^2 + v_o t \quad (13)$$

where, $i \geq 2$, x_j^i is represented as the location of the i^{th} follower slalp in the j^{th} dimension, $v = \frac{x-x_o}{t}$, $a = \frac{v_{final}}{v_o}$, v_o is indicated as initial speed, and t is represented as time. By considering $v_o = 0$, the Equation is updated and represented as:

$$x_j^i = 1/2(x_j^i + x_j^{i-1}) \quad (14)$$

The fitness function of this study is mentioned in Equation (15). The pseudocode of the conventional SSA and conventional SSA for phase optimization is given below:

$$fitness = min(PAPR) \quad (15)$$

Salp Swarm Algorithm (SSA) for optimization.

Algorithm Steps:

Initialization:

Salps of a specific population are formed. we apply this method to create a set of salps where each salp is a candidate solution to the problem concerning optimization, salps population x_i , $i = 1, 2, 3, \dots, n$ by fixing ub and lb values.

Iteration Loop:

The loop runs until a predefined termination condition is reached (maximum number of iterations, permissible degree of fitness, etc.).

Within each iteration:

Fitness Evaluation: The fitness of each salp (solution) is thus defined according to the optimization problem in focus.

Best Search Agent (BSA) Identification: The salp with the highest fitness value on the problem space is selected as the new BSA (leader).

Position Update:

Leader Update: What is done with the leader is updating its position with a levy flight equation (like the one shown in Equation (11)). This promotes exploration.

Follower Update: Each follower changes its position by adding a distance proportional to its distance to the leader, a distance to its previous position, and some random movement. This formula is similar to the one in Equation [14]. It is a form of balancing exploration and exploitation at the same time.

Parameter Adjustment:

When all salp positions are updated, new ones are determined, first by the given control parameters (λ and ω) to stabilize the algorithm.

Termination and Output:

Finally, there is the loop-stopping condition or criterion upon which the loop stops running.

The best fitness value in the population belongs to the BSA, denoting the leader of the SSA algorithm who attains the best optimal solution closer to the global optimum solution.

Phase Optimization with SSA:

The pseudocode presented appears to be a variant of the typical SSA where the labels and numbers in the code refer to ‘phase optimization’ of a special problem of interest; The rest of the structure of the code appears very similar to SSA; The fitness function and possibly the position update equations, such as Equation (15), may change depending on the problem of interest and the variables involved in phase optimization to suit the special problem of interest.

In ISSA, a dynamic weight element is incorporated with w the SSA to control the global and local search ability of the population. The Equation (14) is updated and it is stated in Equation (16). The dynamic weight element w_l is

mathematically expressed in Equation (17).

$$x_j^i = \frac{1}{2} \times w_l \times (x_j^i + x_j^{i-1}) \tag{16}$$

$$w_l = w_{max} \times c_4 - \left(\frac{l}{L}\right) \times (w_{max} - w_{min}) \tag{17}$$

where, w_l is represented as the weight element of l^{th} iteration, w_{max} and w_{min} are denoted as the upper and lower limits of the dynamic weight element w , which ranges between w zero to one. In addition, a Levy flight process is employed in conventional SSA to improve the optimization algorithm’s global exploration ability by combining the short walks route with long jumps to search the solution space. The Levy flight process updates the population position, and it is mathematically specified as follows:

$$x_j^i(l + 1) = 1/2 \times w_l \times (x_j^i(l) + S \oplus x_j^{i-1}(l)) \tag{18}$$

where, $x_j^i(l + 1)$ is indicated as the position of the populations after performing Levy flight operation, $x_j^i(l)$ is represented as the current population position, S is stated as a random step, which obeys the Levy distribution, and the dot product between elements is denoted as \oplus .

The levy flight process combines small steps with occasional larger jumps, allowing for compelling solution space exploration. The optimization algorithm avoids getting stuck in local minima, improving its global search capability.

The dynamic weight element w_l plays a crucial role in balancing the algorithm between exploration and exploitation. The range of w_l , constrained between 0 and 1, ensures smooth control over this balance across iterations.

The steps involved in ISSA for phase optimization are mentioned below:

ISSA for Phase Optimization:

Initialization:

Describe the initial setting of all of the “salps” (population members) in the search space.

Define the number of run cycles of the algorithm to be conducted expressed in terms of the maximum number of iterations.

Define the population objective (the number of salps you want).

Fitness Evaluation:

Coming up with an average fitness value for each of the salp meeting the optimization problem we have at hand is phase optimization in this case. Find the salp with the high fitness value. This salp shows the current solution as the “food source,” or let us call it the first guess for the best solution.

Position Update:

Move all salps in the population through a time step while keeping the next positions unknown by other salps.

The salp (salp with the best performance) moves according to Equation (7) so that the algorithm can efficiently search the wide area.

Lag follower salps reposition according to Equation (18), assuming the leader’s location and the salp’s previous coordinates.

Fitness Re-evaluation:

If the positions of all salps are changed, compute the new fitness values for any new positions.

Food Source Update:

This can be done by comparing the newly calculated fitness value with the current position of the food source and the present solution.

This Equation is used to set the new food source position to be the position of the salp. This ensures that as the iterations proceed more and more, the algorithm gets there closer to the optimal phase solution.

Iteration Loop:

If the main loop gets the return value “false,” return to position update until the maximum number of iterations is reached. The assumed parameters of the ISSA are: number of iterations is 50, population size is 40, w_{min} is 0.4, w_{max} is 0.9, ub is 0.9 and lb is 0.4.

B. SECOND PROPOSED SYSTEM (ISPR-OTFS)

This section presents the ISPR technique, an innovative approach to reducing the PAPR. This technique aims to simplify the usual PTS method [28] and eliminate the requirement for conveying side information, as seen in Figure 3. As seen in Figure 4, the ISPR technology operates in the following manner: The OTFS signal and preset phase sequence are separated into n sub-blocks, as shown in Equation (19).

In Figure 5, each sub-block of the OFDM signal of N/n elements (S_n) is then element-wise multiplied by the corresponding sub-block phase sequences of N/n elements

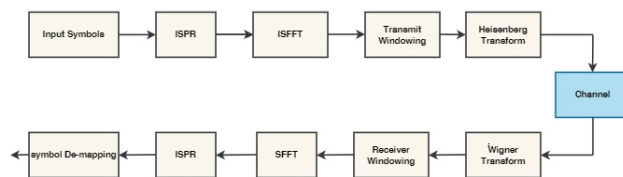


FIGURE 3. Flow diagram of the ISPR-OTFS system.

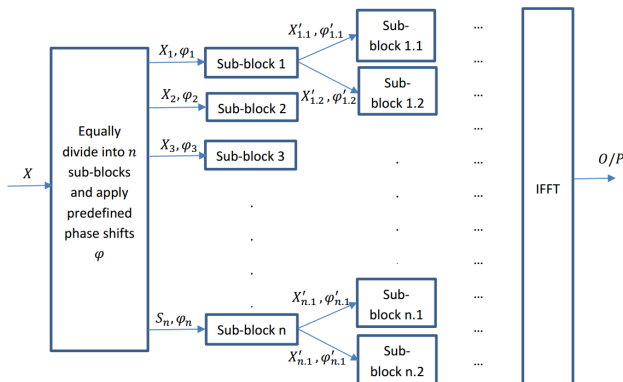


FIGURE 4. Flow diagram of ISPR technique.

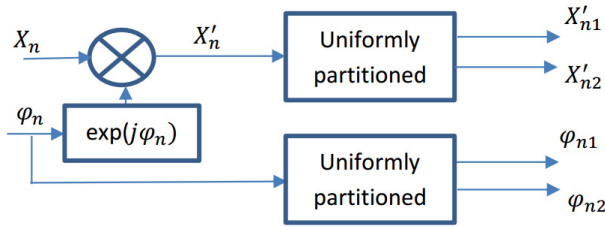


FIGURE 5. Sub-block diagram.

as in (20), where N is the number of subcarriers.

$$X = [X_1, X_2, X_3, \dots, X_n], \quad \varphi = [\varphi_1, \varphi_2, \varphi_3, \dots, \varphi_n] \tag{19}$$

$$X'_i = X_i \cdot \exp(j \cdot \varphi_i) \quad \text{where } i = 1, 2, 3, \dots, n \tag{20}$$

Next, each of the resulting sub-block X'_i and φ_i the sub-block of φ_i are further divided into 2 sub-groups S'_{i1} and S'_{i2} of $(N/n)/2$ elements and φ_{i1} and φ_{i2} as in (21), respectively. Each is then element-wise multiplied by a corresponding division of the predefined phase sequences as in (22). The process is repeated until each group contains only one element (subcarrier), where the resulting signal has a lower PAPR than the original OFDM signal.

$$X'_i = [X'_{i1}, S'_{i2}], \quad \varphi_i = [\varphi_{i1}, \varphi_{i2}] \tag{21}$$

$$X''_{i1} = X'_{i1} \cdot \exp(j \cdot \varphi_{i1}), \quad X''_{i2} = X'_{i2} \cdot \exp(j \cdot \varphi_{i2}) \tag{22}$$

In the receiver, where the inverse process is carried out, each sub-block is multiplied by a conjugate of its same phase factor used at the transmitter in reverse order until the original OFDM signal is recovered, as in (23) and (24).

$$Y'_{i1} = Y''_{i1} \cdot \exp(-j \cdot \varphi_{i1}), \quad R'_{i2} = Y''_{i2} \cdot \exp(-j \cdot \varphi_{i2}) \tag{23}$$

$$Y_i = Y'_i \cdot \exp(-j \cdot \varphi_i) \tag{24}$$

The pseudocode of the ISPR is shown in Algorithm 1. The algorithm receives a signal, an initial group size, and an optional set of phases as its input. The algorithm produces the processed signal and phases as its output. If no phases are specified, the method will produce random phases that are the same length as the signal. The technique applies phase rotations to sub-blocks of the signal in an iterative manner. The group size begins with the starting group size and is divided in half in each iteration until it reaches a size of 1. The method calculates the number of subblocks during each iteration by considering the signal's length and the current group size.

The algorithm calculates the phase for each subblock by using the phases corresponding to the subblock's starting and ending indices. The computed phase is subsequently utilized to modify the signal by applying the phase function. Once all the subblocks have been processed, the group size is reduced by half, and the algorithm proceeds to the next iteration. Ultimately, the method produces the treated signal as its output and the phase vector employed for rotation.

Algorithm 1 Iterative Sub-Block Phase Rotation (ISPR)

1. Input:
 - *input_signal*: The original signal to be processed.
 - *initial_group_size*: The starting size of groups for phase rotation.
 - *phases_input*: An optional array of phase values.
2. Output:
 - *output_signal*: The signal after phase rotation.
 - *phases_used*: The array of phase values applied to the signal.
3. Initialize:
 - Set *group_size* to *initial_group_size*.
 - Set *output_signal* to *input_signal*.
4. Check Phase Input:
 - If *phases_input* is not provided:
 - Generate random phase values of the same length as *input_signal*.
 - Else
 - Use the provided *phases_input* as *phases_used*.
5. Iterative Phase Rotation:
 - While *group_size* is greater than 1:
 - Compute the number of sub-blocks as the length of *input_signal* divided by *group_size*.
 - For each sub-block i (from 0 to *num_subblocks* - 1):
 - Calculate the start and end indices of the current sub-block:
 - $start_index = i * group_size$
 - $end_index = (i + 1) * group_size$
 - Determine the phase to apply using the segment of *phases_used* corresponding to this sub-block:
 - $current_phase = \text{compute phase from } phases_used[start_index : end_index]$
 - Apply the computed phase to *output_signal* within the sub-block indices.
 - Reduce the *group_size* by half for the next iteration.
6. Return:
 - *output_signal*, *phases_used*

V. SIMULATION RESULTS

The proposed methods for OTFS were implemented and analyzed using Matlab- 2018. The assumed parameters of the system are represented in Table 1 [28]. The numerical simulation is carried out to measure the effectiveness of the systems. Here, 20,000 symbols are randomly created, modulated by 256 QAM, and used to evaluate the effectiveness of the systems on the Rayleigh channel with AWGN. The exhaustive search in the systems significantly obtains Optimal Phase Factors (OPFs). By increasing the number of partitions, it is observed that the PAPR value is reduced in the proposed systems.

In Fig. 6, we analyzed the performance of the first proposed hybrid and conventional algorithms for OTFS waveforms with 256 subcarriers. The main objective was to determine the optimal PAPR obtained at a 10^{-3} CCDF. The PAPR reduction equal 0.5 dB, 2.2 dB, 3.3 dB, 4.3 dB, 4.8 dB,

TABLE 1. Simulation parameters.

Parameter	Value
Number of Subcarriers	256
Subcarrier Spacing	15Khz
Modulation Type	256 QAM
Number of Particles	50
Number of Paths	9
Channel type	Rician channel with AGWN
Number of iterations	25
Number of subblocks	4, 8, 64
Number of bits	100000

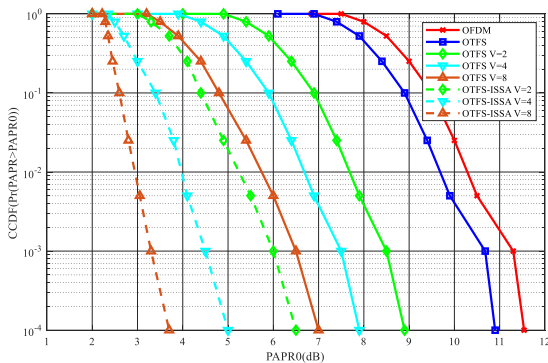


FIGURE 6. PAPR reduction with the proposed system.

6.1 dB, and 8 dB were obtained by the conventional OTFS, PTS $v = 4$, PTS $v = 8$, PTS $v = 64$, PTS-ISSA $v = 4$, PTS-ISSA $v = 8$, and PTS-ISSA $v = 64$ as compared with the traditional OFDM. The suggested algorithm and PTS-ISSA produced better results and performed better than the conventional approaches. By adding more sub-blocks, the PAPR reduction was further enhanced. On the other hand, adding more sub-blocks could make the system more complex. PAPR analysis in Rician channels is essential for effective power amplifier design in mobile communications. It assists in anticipating infrequent, high-power signal peaks brought on by the channel, helping to avoid expensive clipping and distortion.

This results in faster data rates without using more spectrum, which is essential for enabling various 5G applications and raising the framework's PAPR. Therefore, it can be said that the hybrid algorithms that have been suggested achieve the best PAPR performance. Because there are more opportunities for constructive interference, the Rician channel mimics a typical dispersed mobile environment with random signal fluctuations and a higher likelihood for severe peaks in 256 subcarriers. PAPR analysis is essential for both possible PAPR reduction strategies and amplifier design.

Figure 7 shows comparing the PAPR reduction of the ISPR to conventional techniques. It is seen that at the CCDF of 10^{-3} , the PAPR reduction of 5.1 dB, 7.2 dB, and 8.2 dB were obtained by ISPR-OTFS $v = 4$, ISPR-OTFS $v = 8$, and ISPR-OTFS $v = 64$ as compared with the conventional OFDM.

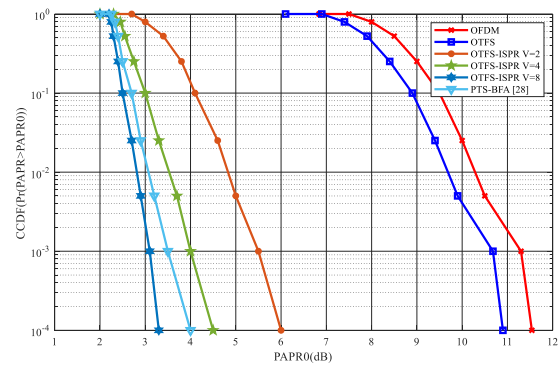


FIGURE 7. PAPR reduction with the OTFS-ISPR system.

The PAPR reduction achieved by ISSA-PTS and ISPR-OTFS systems shows significant improvements over the BFA-PTS method [28]. Specifically, the ISSA-PTS system achieved a 2.56% improvement in PAPR reduction, while the ISPR-OTFS system demonstrated a 5.13% improvement over BFA-PTS, with a PAPR reduction of 8.2 dB. Also, PTS-BFA in [28] reduces by 7.8 dB.

The ISPR-OTFS technique demonstrates superior performance regarding PAPR reduction compared to the ISSA-OTFS approach. The improvements achieved by ISPR-OTFS range from 6.06% to 7.84% across different sub-block configurations, highlighting its effectiveness in reducing the peak-to-average power ratio more efficiently than ISSA-OTFS.

The 5 G's OTFS waveforms' decreased PAPR increases the BER. There is a trade-off here between possible signal deterioration and amplifier efficiency. In addition to introducing small signal alterations that could raise the BER value and deteriorate the framework's performance, the PAPR approach lowers the peaks for amplifier safety. Therefore, examining the framework's throughput performance for the suggested algorithms in Rician channel scenarios is crucial. The primary goal is to reduce the PAPR while maintaining the OTFS's BER performance.

Fig. 8 displays a BER analysis of the Rician channels for the 256 subcarriers. Thus, it can be said that the suggested approaches effectively maintain the framework's BER.

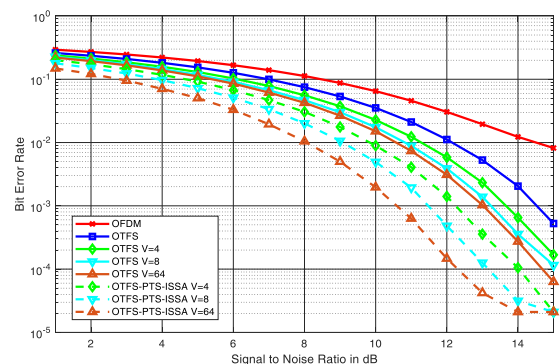


FIGURE 8. BER of the OTFS-PTS-ISSA system.

Therefore, it can be said that the suggested hybrid approach effectively raised the framework's performance. Consequently, the findings show that the proposed methods preserve BER performance while lowering the framework's PAPR.

Fig. 8 illustrates the analysis of the BER performance for an OTFS waveform under the influence of a Rician Channel utilizing 256 subcarriers. It is seen that at the BER of 10^{-2} , the SNR of 2.5 dB, 3.2 dB, 3.5 dB, 3.6 dB, 4.5 dB, 5.1 dB, and 6.5 dB were obtained by the conventional OTFS, PTS $v = 4$, PTS $v = 8$, PTS $v = 64$, PTS-ISSA $v = 4$, PTS-ISSA $v = 8$, and PTS-ISSA $v = 64$ as compared with the traditional OFDM. Hence, it is concluded that the proposed PTS-ISSA $v = 8$ outperforms the conventional and contemporary algorithms.

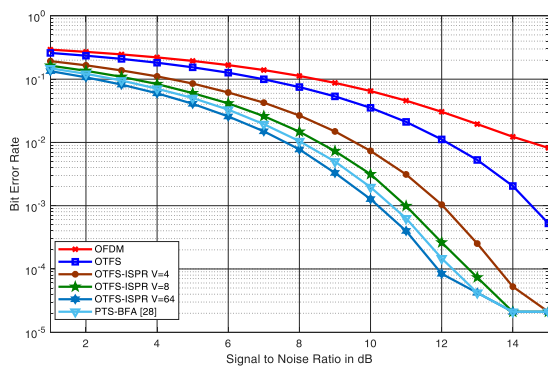


FIGURE 9. BER of the OTFS-ISPR system.

As a result, the BER performance was successfully maintained using the suggested approach. By dispersing signal energy over time and frequency, OTFS waveforms are intended to increase the durability of Rician channels. The proposed hybrid algorithms can further strengthen this resistance. Nevertheless, the channel conditions determine their influence on the power spectrum density, which is associated with the dispersion of signals across frequencies.

Fig. 9 illustrates the BER performance for the OTFS-ISPR system. It is seen that at the BER of 10^{-2} , the SNR of 4.8 dB, 5.5 dB, and 6.9 dB were obtained by PTS $v = 4$, PTS $v = 8$, PTS $v = 64$, PTS-ISSA $v = 4$, PTS-ISSA $v = 8$, and PTS-ISSA $v = 64$ as compared with the conventional OFDM.

ISPR-OTFS also outperforms ISSA-OTFS, with improvements ranging from 6.15% to 7.84%, depending on the sub-block configuration. This indicates that ISPR-OTFS reduces PAPR more effectively and maintains better bit error rate performance, making it a more robust solution for communication systems.

In terms of BER performance, the ISSA-PTS system showed a 1.56% improvement in SNR compared to BFA-PTS, achieving an SNR of 6.5 dB at a BER of 10^{-2} . The ISPR-OTFS system achieved a 7.81% improvement in SNR over BFA-PTS, with an SNR of 6.9 dB, indicating superior performance in both PAPR and BER reduction.

Because of the structural differences in the other advanced waveforms, the traditional PAPR methods employed in OFDM cannot be applied to them. As such, a specific waveform design must inform the implementation of a distinct PAPR algorithm. Additionally, to the best of our knowledge and the literature that is currently accessible, the proposed study is the first to apply hybrid algorithms like PTS-ISSA for PAPR reduction in the OTFS waveform. Recent studies have shown that decreasing complexity and PAPR results in a decrease in BER performance.

This study focuses on Rician channels, which are highly relevant for scenarios with a strong line-of-sight (LOS) component, such as urban and vehicular communication systems. A dominant LOS signal in Rician fading channels introduces occasional high-power peaks, making PAPR reduction essential to ensure efficient power amplifier design and prevent signal distortion. Our proposed hybrid algorithms, ISSA-PTS and ISPR-OTFS, are optimized for these conditions, balancing PAPR reduction and BER performance in high-mobility environments.

A. COMPLEXITY

Because of the structural differences in the other advanced waveforms, the traditional PAPR methods employed in OFDM cannot be applied to them. As such, a specific waveform design must inform the implementation of a distinct PAPR algorithm. Additionally, to the best of our knowledge and the literature that is currently accessible, the proposed study is the first to apply hybrid algorithms like PTS-ISSA for PAPR reduction in the OTFS waveform. ISPR with 4 sub-blocks requires an extra multiplication process than ISPR with 8, 64 sub-blocks, which, in turn, has more significant computational complexity. Therefore, the initial sub-block division of 4 is a good candidate in practice. Recent studies have shown that decreasing complexity and PAPR decreases BER performance; however, in this work, we find that the BER performance is maintained for 256 subcarriers without affecting PAPR performance.

The computational complexity of the proposed ISSA-PTS and ISPR-OTFS methods is significantly lower than that of traditional PTS, with ISSA-PTS decreasing complexity to $O(v \cdot n_{iter})$ by optimizing the search process using fewer iterations, and ISPR-OTFS achieving linear complexity $O(v)$, making both methods more scalable and efficient for real-time applications compared to the exponential complexity $O(2^v)$ of conventional PTS. This reduced complexity makes ISSA-PTS and ISPR-OTFS more available for hardware implementation on FPGAs and GPUs, which can exploit the parallelism of these algorithms. Both methods, especially ISPR-OTFS, are ideal for large-scale communication systems like 5G due to their scalability and reduced computational overhead. The lower iteration count of ISSA-PTS improves parallel processing performance, while ISPR-OTFS's linear complexity makes it adaptable to real-time applications where latency and power efficiency are crucial. These methods balance computational efficiency and high performance

by minimizing iterations and simplifying the search process, making them feasible for next-generation communication networks.

VI. CONCLUSION

This study addresses the critical challenge of PAPR reduction in OTFS systems, particularly in high-mobility environments, and satellite. The proposed hybrid ISSA-PTS and ISPR techniques significantly improve both PAPR and BER performance, providing robust solutions to enhance communication reliability. ISSA-PTS employs advanced optimization to minimize PAPR and reduce signal distortion, while ISPR offers a scalable, efficient strategy that maintains BER performance with less complexity. Simulation results validate the effectiveness of these techniques, highlighting their potential for practical OTFS applications.

For future work, we plan to explore real-time hardware implementation of the proposed algorithms on platforms like FPGAs and GPUs, further optimize their computational complexity, and evaluate their performance in MIMO OTFS systems. Additionally, we aim to assess their effectiveness in other fading models, such as Nakagami-m, and explore their applicability in 6G networks, particularly in high-frequency bands and massive MIMO systems. These directions will further enhance the scalability and practicality of the proposed methods for next-generation wireless networks.

REFERENCES

- [1] Z. Wei, W. Yuan, S. Li, J. Yuan, G. Bharatula, R. Hadani, and L. Hanzo, "Orthogonal time-frequency space modulation: A promising next-generation waveform," *IEEE Wireless Commun.*, vol. 28, no. 4, pp. 136–144, Aug. 2021.
- [2] K. K. Vaigandla and G. Balakrishna, "Evaluation of PAPR, PSD, spectral efficiency, BER and SNR performance of multi-carrier modulation schemes for 5G and beyond," *Int. J. Electr. Electron. Eng.*, vol. 10, no. 11, pp. 100–114, Nov. 2023.
- [3] A. Kumar, N. Gaur, S. Chakravarty, and A. Nanthaamornphong, "Reducing the PAPR of OTFS modulation using hybrid PAPR algorithms," *Wireless Pers. Commun.*, vol. 133, no. 4, pp. 2503–2523, Dec. 2023.
- [4] S. Jaffry, R. Hussain, X. Gui, and S. F. Hasan, "A comprehensive survey on moving networks," *IEEE Commun. Surveys Tuts.*, vol. 23, no. 1, pp. 110–136, 1st Quart., 2021.
- [5] S. Li, J. Yuan, W. Yuan, Z. Wei, B. Bai, and D. W. K. Ng, "Performance analysis of coded OTFS systems over high-mobility channels," *IEEE Trans. Wireless Commun.*, vol. 20, no. 9, pp. 6033–6048, Sep. 2021, doi: 10.1109/TWC.2021.3071493.
- [6] M. Zhou, F. Chen, H. Yu, and J. Lu, "Iterative channel estimation for OTFS systems based on low-PAPR hybrid superimposed pilots," *IEEE Commun. Lett.*, vol. 28, no. 8, pp. 1939–1943, Aug. 2024.
- [7] S. Sharma, S. Waqas Haider Shah, and J. Widmer, "A low-complexity standard-compliant PAPR reduction scheme for OTFS modulation," in *Proc. IEEE 99th Veh. Technol. Conf. (VTC-Spring)*, Jun. 2024, pp. 1–7.
- [8] L. Gaudio, G. Colavolpe, and G. Caire, "OTFS vs. OFDM in the presence of sparsity: A fair comparison," *IEEE Trans. Wireless Commun.*, vol. 21, no. 6, pp. 4410–4423, Jun. 2022.
- [9] A. Kumar, S. Chakravarty, and A. Nanthaamornphong, "Analysis of PAPR reduction of optical-OTFS for 256-QAM using companding and clipping-filtering algorithms," *J. Opt. Commun.*, vol. 1, pp. 1–26, Jan. 2024.
- [10] Q. Guo, Z. Yuan, F. Liu, and J. Yuan, "OTFS and delay-Doppler domain modulation: Signal detection and channel estimation," in *Signals and Communication Technology*. Cham, Switzerland: Springer, 2024, pp. 187–225.
- [11] Z. Sui, H. Zhang, Y. Xin, T. Bao, L.-L. Yang, and L. Hanzo, "Low complexity detection of spatial modulation aided OTFS in doubly-selective channels," *IEEE Trans. Veh. Technol.*, vol. 72, no. 10, pp. 1–6, Apr. 2023.
- [12] A. M. Graff, W. N. Blount, P. A. Iannucci, J. G. Andrews, and T. E. Humphreys, "Analysis of OFDM signals for ranging and communications," in *Proc. GNSS*, Oct. 2021, pp. 2910–2924.
- [13] J. Shi, X. Hu, Z. Tie, X. Chen, W. Liang, and Z. Li, "Reliability performance analysis for OTFS modulation based integrated sensing and communication," *Digit. Signal Process.*, vol. 144, Jan. 2024, Art. no. 104280.
- [14] W. Yuan, S. Li, Z. Wei, Y. Cui, J. Jiang, H. Zhang, and P. Fan, "New delay Doppler communication paradigm in 6G era: A survey of orthogonal time frequency space (OTFS)," *China Commun.*, vol. 20, no. 6, pp. 1–25, Jun. 2023.
- [15] A. A. M. Khalaf, M. Elnabawy, and N. Azzam, "Non-linear companding techniques with ACO-ofdm-based VLC systems for PAPR reduction," *J. Adv. Eng. Trends*, vol. 42, no. 2, pp. 53–69, Jul. 2023.
- [16] J. Su, S. Liu, Y. Huang, and J. Yuan, "Peak-to-average power ratio reduction via symbol precoding in OTFS modulation," in *Proc. IEEE 95th Veh. Technol. Conf.*, Jun. 2022, pp. 1–5.
- [17] G. M. Salama, Y. S. Mohamad, and M. T. Saif, "The role of sigma-delta ADCs and zero-forcing estimator in massive MIMO channel estimation," *J. Adv. Eng. Trends*, vol. 43, no. 2, pp. 445–454, Jun. 2024.
- [18] S. Chennamsetty, S. Boddu, P. Chandhar, and K. C. Bulusu, "Analysis of PAPR in OTFS modulation with classical selected mapping technique," in *Proc. 15th Int. Conf. Commun. Syst. Netw. (COMSNETS)*, Jan. 2023, pp. 319–322.
- [19] A. Kumar, S. Chakravarty, C. Sao, T. M. Syed, and A. Nanthaamornphong, "Peak to average power ratio Est. and analysis in OTFS 6G waveform by using selective mapping algorithm," in *Proc. SoutheastCon*, Mar. 2024, pp. 1070–1074.
- [20] A. S. Sümer, T. Yilmaz, E. Memisoglu, and H. Arslan, "Exploiting OTFS frame structure for PAPR reduction," in *Proc. IEEE 96th Veh. Technol. Conf. (VTC-Fall)*, Sep. 2022, pp. 1–5.
- [21] A. K. Abed, R. Mansoor, and A. K. Abed, "Particle swarm optimization-based dummy sub-carriers insertion for peak to average power ratio reduction in OFDM systems," *ICT Exp.*, vol. 8, no. 1, pp. 135–141, Mar. 2022.
- [22] H. Bitra and N. Raj, "OTFS: PAPR reduction using nonlinear companding transform," *Int. J. Electron. Lett.*, vol. 12, no. 3, pp. 281–294, Jul. 2024.
- [23] M. Alaa, G. Salama, A. Galal, and H. Hamed, "A robust lane detection method for urban roads," *J. Adv. Eng. Trends*, vol. 41, no. 1, pp. 13–26, Jan. 2022.
- [24] G. M. Salama, H. F. Abdalla, A. A. Mohamed, E. S. Hassan, M. I. Dessouky, A. A. M. Khalaf, A. El-Emary, and A. S. Elsafrawy, "PAPR reduction technique for FBMC based visible light communication systems," *IET Commun.*, vol. 16, no. 15, pp. 1807–1814, Sep. 2022.
- [25] G. M. Salama, A. A. Mohamed, and H. F. Abdalla, "Evaluating DNN and LSTM nonlinear compensators for enhanced performance in DCO-OFDM system," *J. Opt. Commun.*, vol. 2, pp. 1–26, Jan. 2024.
- [26] R. A. Roshdy, A. I. Hussein, M. M. Mabrook, and M. A. Salem, "A complexity efficient PAPR reduction scheme for FBMC-based VLC systems," *Opto-Electron. Rev.*, vol. 3, May 2023, Art. no. e144919.
- [27] A. A. A. Wahab, N. Q. M. Adnan, S. S. N. Alhady, and W. A. F. W. Othman, "Particle swarm optimization for PAPR reduction of OFDM systems," in *Proc. Symp. Intell. Manuf. Mechatronics*, 2023, pp. 815–826.
- [28] A. Kumar, N. Gaur, and A. Nanthaamornphong, "Optimizing PAPR, BER, and PSD efficiency: Using phase factors generated by bacteria foraging algorithm for PTS and SLM methods," *IEEE Access*, vol. 12, pp. 54964–54977, 2024.
- [29] S. Taba, S. Redadaa, M. A. Benchana, and S. Ikni, "A low-complexity PTS technique-based improved PSO algorithm for PAPR reduction in OFDM systems," *Telecommun. Radio Eng.*, vol. 82, no. 8, pp. 1–17, 2023.
- [30] F. Hu, H. Xu, L. Jin, J. Liu, Z. Xia, G. Zhang, and J. Xiao, "Continuous-unconstrained and global optimization for PSO-PTS based PAPR reduction of OFDM signals," *Phys. Commun.*, vol. 55, Dec. 2022, Art. no. 101825.
- [31] S. Mirjalili, A. H. Gandomi, S. Z. Mirjalili, S. Saremi, H. Faris, and S. M. Mirjalili, "Salp swarm algorithm: A bio-inspired optimizer for engineering design problems," *Adv. Eng. Softw.*, vol. 114, pp. 163–191, Dec. 2017.
- [32] H. Pradhan, B. B. Mangaraj, and S. K. Behera, "Improved salp swarm optimization based circular arrays in presence of mutual coupling," *Int. J. RF Microw. Comput.-Aided Eng.*, vol. 31, no. 8, pp. 1–22, Aug. 2021.



GERGES MANSOUR SALAMA received the B.Sc. degree in electrical engineering and the M.Sc. degree in electronics and communications engineering from El-Minia University, El-Minia, Egypt, in 1999 and 2006 respectively, and the Ph.D. degree from the Faculty of Telecommunication Networks, Switching Systems, and Computer Technology (FTN, SS, and CT), St. Petersburg State University of Telecommunications Prof. M. A. Bonch-Bruевич, Ministry of Communications and Mass Media of the Russian Federation Federal Communications Agency, in 2012. He is currently an Associate Professor with the Faculty of Engineering, Minia University, Egypt. His current research interests include image enhancement, image restoration, image interpolation, super-resolution reconstruction of images, data hiding, wireless communications systems design, multimedia communications, medical image processing, optical signal processing, and digital communications.

AMIRA A. MOHAMED received the B.Eng. and M.Sc. degrees in electrical and communications engineering from Al-Azhar University, Cairo, Egypt, in 2012 and 2020, respectively. She is currently pursuing the Ph.D. degree with the Faculty of Engineering, Minia University, Egypt, with a focus on “Performance Enhancement of Multicarrier Modulation Techniques Based VLC Systems and Machine Learning.” She is also an Assistant Lecturer at the Higher Institute of Engineering and Technology, Kafr El-Sheikh. Her current research interests include performance enhancement of OFDM in visible light communication systems, machine learning, and deep learning applications in telecommunications, the IoT, AI, and network security.



AZIZA I. HUSSEIN (Member, IEEE) received the B.Sc. and M.Sc. degrees from Assiut University, Egypt, in 1983 and 1989, respectively, and the Ph.D. degree in electrical and computer engineering from Kansas State University, Manhattan, KS, USA, in 2001. In 2004, she joined Effat University, Saudi Arabia, and established the first Electrical and Computer Engineering Program for women in the country and taught related courses. She was the Head of the Electrical and Computer Engineering Department, Effat University, from 2007 to 2010. She was the Head of Computer and Systems Engineering Department, Faculty of Engineering, Minia University, Egypt, from 2011 to 2016. She was also a Professor and the Chair of the Department of Electrical and Computer Engineering and the Director of the Master of Energy Program, Effat University, from 2016 to 2021. She is currently a Professor and a Researcher with the Department of Electrical and Computer Engineering, Effat University. Her research interests include microelectronics, analog/digital VLSI system design, RF circuit design, high-speed analog-to-digital converters design, and wireless communications systems design.



M. MOURAD MABROOK received the B.Sc. and M.Sc. degrees in electrical and communication engineering from Assiut University, Egypt, in 2008 and 2013, respectively, and the Ph.D. degree from the Communication Department, Menia University, Egypt, in 2017. Since 2021, he has been the Head of the Applied Sciences of Space and Navigation Program. He is currently an Associate Professor with the Space Communication Engineering Department, Faculty of Navigation Science and Space Technology (NSST), Beni-Suef University, Beni Suef, Egypt. He is also a part-time Assistant Professor with the Faculty of Engineering, Nahda University (NUB), Beni Suef. His research interests include wireless communications, 5G networks, cognitive radio, artificial intelligence, circuit design, and sensors. He has published more than 30 journals and conference papers in the above fields. He is a reviewer of many international journals related to Elsevier, Springer, and IEEE Publishers’.

• • •